Eur. Phys. J. B **29**, 385–398 (2002)
DOI: 10.1140/epjb/e2002-00322-7

THE EUROPEAN PHYSICAL JOURNAL B

Dynamics of modulated and composite aperiodic crystals

The signature of the inner polarization in the neutron coherent inelastic scattering

O. Radulescu[1], T. Janssen[2], and J. Etrillard[3,4,a]

[1] Institut de Recherche Mathématique de Rennes, University of Rennes 1, Campus de Beaulieu, 35042 Rennes, France
[2] Institute of Theoretical Physics, Nijmegen University, Postbus 9010, 6500 GL Nijmegen, The Netherlands
[3] Groupe Matière Condensée et Matériaux, University of Rennes 1, Campus de Beaulieu, 35042 Rennes, France
[4] Laboratoire Léon Brillouin, CEA-CNRS-CE Saclay, 91191 Gif-sur-Yvette, France

Received 9 June 2002
Published online 14 October 2002 –

Abstract. We compare within an unifying formalism the dynamical properties of modulated and composite aperiodic (incommensurate) crystals. We discuss the concept of inner polarization and we define an inner polarization parameter β that distinguishes between different acoustic modes of aperiodic crystals. Although this concept has its limitations, we show that it can be used to extract valuable information from neutron coherent inelastic scattering experiments. Within certain conditions, the ratio between the dynamic and the static structure factors at various Bragg peaks depends only on β. We show how the knowledge of β for modes of an unknown structure can be used to decide whether the structure is composite or modulated. The same information can be used to predict scattered intensity within unexplored regions of the reciprocal space, being thus a guide for experiments.

PACS. 61.44.-n Semiperiodic solids – 63.20.Dj Phonon states and bands, normal modes, and phonon dispersion – 61.12.-q Neutron diffraction and scattering

1 Introduction

Aperiodic crystals are long-range ordered structures whose diffraction patterns are made of Bragg peaks. The difference with respect to normal crystals is that they are not periodic and one needs $n = 3 + D$ (D is the dimension of the internal space) basis vectors to index the positions of peaks in reciprocal space:

$$\mathbf{q} = \sum_{i=1}^{n} z_i \mathbf{q}_i, \; z_i \in \mathbb{Z}. \tag{1}$$

This property has been exploited in crystallography by embedding the structure in a superspace crystal of dimension n. Atomic positions are the intersections between the D-dimensional atomic surfaces and the 3-dimensional physical space. For periodic crystals, the Floquet-Bloch theory reduces the $3N$ dimensional eigenvector problem of lattice modes (N is the number of atoms) to a $3N_u$ dimensional problem (N_u being the number of atoms inside the unit cell). The similar approach can be used for aperiodic crystals, but in this case the number of equations is not reduced; because of incommensurability $N_u = N$. Nevertheless, as we show in this paper, superspace concepts lead to important simplifications in the description of modes, that can be used in the analysis of inelastic neutron scattering experiments.

At present, three classes of aperiodic crystals are known: incommensurate modulated crystals, incommensurate composites and quasicrystals [1–4]. Atomic surfaces are discontinuous for quasicrystals, but they can be continuous for modulated crystals and for composites. The borders between the three classes are not so clear as one may think. The classification difficulties between modulated and composites crystals are notorious. If discontinuous atomic surfaces and occupational modulations are allowed [5,6], any modulated structure can be seen as a composite one and *vice versa*. The choice can be particularly difficult in compounds with a complex structure. For instance, recent structural neutron investigations of Bi-2212 superconductors [7] emphasize the difficulty of deciding whether these materials should be called composite or modulated. A natural question arises. Can dynamics as probed by inelastic neutron scattering experiments [9,10] give an answer to this classification problem?

In order to answer this question we need to know the typical dynamical responses of different aperiodic crystals. Several simplified model systems will be investigated, hoping that more complex systems behave in resemblance to one of these. Of course, it is also possible that compounds that structurally are at the border between the

[a] e-mail: Ovidiu.Radulescu@univ-rennes1.fr

three classes of aperiodic crystals have also special dynamical properties, at the border between the ones studied here, in which case the classification problem could be really intractable.

In this paper, we discuss the linear (small amplitude) excitations of displacively modulated and composite crystals. The case of occupational modulations and that of non-linear (large amplitude) excitations will be studied elsewhere.

We focus our discussion on the dynamics of low frequency excitations. The n-dimensional superspace picture suggests that aperiodic crystals have n branches of propagating hydrodynamic modes. Only three of those are true Goldstone modes, associated to the broken translation symmetry of the Hamiltonian. These three branches are the general acoustic phonons, present in any solid. The other p branches are called phasons because they are associated to the broken "phase" symmetry of the ground states manifold (which is not a symmetry of the Hamiltonian).

The hydrodynamics of composite aperiodic crystals has already been the object of several theoretical papers [11–14]. Although they offer rather complete results (including damping) these papers suffer from their generality and from the use of various phenomenological parameters. It is difficult to extract from them the consequences of incommensurability on dynamics and to find the answers to simple (yet important) questions such as which is the contribution of each mode to the neutron inelastic scattered intensity and which are the regions in the reciprocal space where these contributions are most intense. Modes observability is not only determined by the (integrated) intensity of the peaks, but also by the line shape. The hotly debated problem of damping, whether intrinsic as mode-mode coupling [39] or extrinsic *via* coupling to defects, is left out from our discussion.

The superspace picture suggests that there is a tight connection between structure and dynamics. From the very beginning of our paper we exploit this connection and our purpose is to find a small set of quantities that can be easily interpreted theoretically and measured experimentally, and that facilitate the classification of aperiodic crystals from the point of view of their dynamical properties.

2 Ground states, modulation functions and low frequency excitations

Throughout this paper we shall deal with 1D models, otherwise we shall stay as general as possible.

The positions of the atoms, corresponding to a ground state of a displacively modulated incommensurate crystal, read [2]:

$$\begin{aligned} y_{n,g} &= na_1 + \delta_g + f_g(na_1 + \delta_g) \\ \text{where } & f_g(y + a_2) = f_g(y). \end{aligned} \tag{2}$$

The indexes $n \in \mathbb{Z}, g = 1, n_1$ are for the unit cells of the basic (non-modulated) structure and for the atoms within this unit cell, respectively. f_g are periodic modulation functions of period a_2, a_1 is the period of the basic structure, the ratio $\alpha = a_2/a_1$ is irrational.

A composite has several subsystems. We consider here the simplest case when there are two subsystems. The positions of atoms belonging to the two subsystems read [15]:

$$\begin{aligned} y^{(1)}_{n,g} &= na_1 + \delta^{(1)}_g + f^{(1)}_g(na_1 + \delta^{(1)}_g) \\ y^{(2)}_{m,h} &= ma_2 + \delta^{(2)}_h + f^{(2)}_h(ma_2 + \delta^{(2)}_h) \\ \text{where } & f^{(1)}_g(y + a_2) = f^{(1)}_g(y),\ g = 1, n_1 \\ \text{and } & f^{(2)}_h(y + a_1) = f^{(2)}_h(y),\ h = 1, n_2. \end{aligned} \tag{3}$$

The modulation function of one subsystem has the periodicity that the other subsystem had before modulation.

The ground states of incommensurate modulated and composite crystals are degenerated. This can be explained by the existence of symmetry groups that leave the configuration energy invariant [15]:

– Physical space translations, that are uniform displacements.

$$T_\lambda(y_{n,g}) = y_{n,g} + \lambda \tag{4}$$

$$T_\lambda(y^{(1)}_{n,g}, y^{(2)}_{m,h}) = (y^{(1)}_{n,g} + \lambda, y^{(2)}_{m,h} + \lambda) \tag{5}$$

where $\lambda \in \mathbb{R}$.

– Discrete inner space translations, that are combinations of discrete uniform shifts and relabelling of atomic positions.

$$P_{r,s}(y_{n,g}) = y_{n+r,g} - ra_1 \tag{6}$$

$$P_{r,s}(y^{(1)}_{n,g}, y^{(2)}_{m,h}) = (y^{(1)}_{n+r,g} - ra_1, y^{(2)}_{m+s,h} - ra_1) \tag{7}$$

where[1] $r, s \in \mathbb{Z}$.

The transformations $P_{r,s}$ change the phase of the modulation functions and (only for composites) produce a relative uniform displacement of the subsystems:

$$P_{r,s}(\{na_1 + \delta_g + f_g(na_1 + \delta_g)\}) = \{na_1 + \delta_g + f_g(na_1 + \delta_g + \delta')\} \tag{8}$$

$$\begin{aligned} P_{r,s}(\{&na_1 + \delta^{(1)}_g + f^{(1)}_g(na_1 + \delta^{(1)}_g), \\ &na_2 + \delta^{(2)}_h + f^{(2)}_h(na_2 + \delta^{(2)}_h)\}) = \\ \{&na_1 + \delta^{(1)}_g + f^{(1)}_g(na_1 + \delta^{(1)}_g + \delta'), \\ &na_2 + \delta^{(2)}_h - \delta' + f^{(2)}_h(na_2 + \delta^{(2)}_h - \delta')\} \end{aligned} \tag{9}$$

where the phase variation is:

$$\delta' = ra_1 - sa_2. \tag{10}$$

Physical space and inner space translations have a simple geometrical interpretation in a superspace embedding [15] where they represent uniform translations of the

[1] The action of s is trivial for modulated crystals.

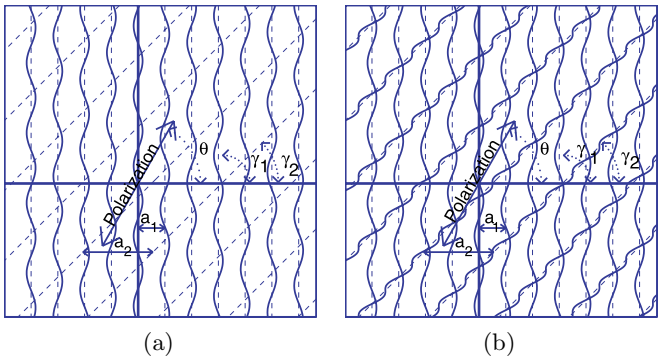

Fig. 1. Superspace embedding of a) modulated incommensurate crystals (one set of atomic surfaces) b) composite incommensurate crystals (two sets of atomic surfaces). For illustration, we have chosen sinusoidal modulation functions. θ is the angle made by the inner polarization and the physical line (horizontal). The inner polarization parameter is $\beta = \tan(\theta)/[2\tan(\gamma_2) - \tan(\theta)]$. The acoustical phonon corresponds to $\theta = 0, \beta = 0$. For composites, modes concentrated on the first subsystem have inner polarization parallel to the atomic surfaces of the second subsystem, *i.e.* $\theta = \gamma_2, \beta = 1$. Modes concentrated on the second subsystem have inner polarization along the atomic surfaces of the first subsystem, *i.e.* $\theta = \gamma_1 = \pi/2, \beta = -1$.

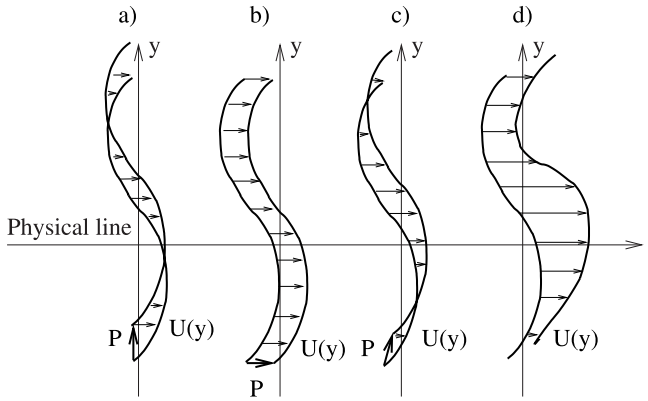

Fig. 2. Different inner polarizations **P** and displacement hull function **U** for modulated crystals; a) phason with **P** $\perp$ **U**, b) acoustical phonon **P**||**U** (**U** is constant), c) mixed phonon/phason, d) distorted atomic surface, inner polarization can not be defined.

superspace crystal. Physical space translations are parallel to the physical space. Inner space translations make a non-zero angle θ with the physical space (Fig. 1). The physical effect of phase translations depends on θ but also on γ_1,γ_2, which are the angles made by basic superspace lattice directions and the physical space. In Figure 1 these lattice directions define the fixed repeat distances a_1 and a_2 along the physical space, while γ_1, γ_2 are free to change. It is convenient to chose $\gamma_1 = \pi/2$. In this case inner space translations defined by equations (8, 9) correspond to $\theta = \pi/2$ (they are orthogonal to the physical space).

More generally, we may define composed translations as combinations $T_\lambda P_{r,s}$ that correspond to translations in superspace along directions making an angle θ with the physical space. If $\gamma_1 = \pi/2$ then one has:

$$\frac{\tan(\theta)}{\tan(\gamma_2)} = \frac{\delta'}{\lambda}\,. \tag{11}$$

Because a_2/a_1 is irrational, the phase variations δ' (Eq. (10)) can approximate with arbitrary precision any real number (they form a dense set). If the modulation functions are smooth (the so-called analytic regime [18]) the group of inner space translations can be extended to a continuous group $\{P_{\delta'}\}_{\delta' \in \mathbb{R}}$ just by using equations (8, 9) previously written for $\delta' = ra_1 - sa_2, r, s \in \mathbb{Z}$ and extend them by continuity to all real values of δ'. Physical space and inner space translations transform ground states into ground states. As a consequence of the $2D$ continuous degeneracy of the ground states manifold there are two hydrodynamic modes. In the limit of infinite wavelength $k \to 0$, the displacements involved by these modes are the infinitesimal physical space and inner space translations [15]:

– Infinitesimal physical space translations

$$u_{n,g} = \epsilon \tag{12}$$

$$\{u^{(1)}_{n,g}, u^{(2)}_{m,h}\} = \{\epsilon, \epsilon\}. \tag{13}$$

– Infinitesimal inner space translations

$$u_{n,g} = \eta \frac{\mathrm{d}f_g}{\mathrm{d}x}(na_1 + \delta_g) \tag{14}$$

$$\{u^{(1)}_{n,g}, u^{(2)}_{m,h}\} = \left\{ \eta \frac{\mathrm{d}f^{(1)}_g}{\mathrm{d}x}\left(na_1 + \delta^{(1)}_g\right), - \eta\left[1 + \frac{\mathrm{d}f^{(2)}_h}{\mathrm{d}x}\left(ma_2 + \delta^{(2)}_h\right)\right]\right\}. \tag{15}$$

Let us define the inner polarization as a vector in superspace: $\mathbf{P} = (\epsilon, \eta\tan(\gamma_2))$. A vibration of the superspace crystal in the direction **P** will correspond to a combination of infinitesimal physical space and inner space translations with coefficients ϵ, η (Fig. 1). The inner polarization should not be understood as the direction of atom displacements (this is the physical polarization, always contained in the physical space), but as a vector belonging to the superspace (abstract construction describing internal degrees of freedom in a geometrical way). When the angle θ between the inner polarization and the physical space changes, it is only the sequence of signs and magnitudes of atom displacements that changes, their direction remaining the same (Fig. 2).

The relation between θ, ϵ, η is analogous to equation (11):

$$\frac{\tan(\theta)}{\tan(\gamma_2)} = \frac{\eta}{\epsilon}\,. \tag{16}$$

Let us define the polarization parameter β as:

$$\beta = \frac{\eta}{2\epsilon - \eta} = \frac{\tan(\theta)}{2\tan(\gamma_2) - \tan(\theta)} \cdot \tag{17}$$

In composites β may be called "sliding parameter" because at $k = 0, \omega = 0$ this is proportional to the relative displacement between the centers of mass of the subsystems.

$$\beta = \frac{\left\langle u^{(1)}_{n,g} \right\rangle - \left\langle u^{(2)}_{m,h} \right\rangle}{\left\langle u^{(1)}_{n,g} \right\rangle + \left\langle u^{(2)}_{m,h} \right\rangle} \tag{18}$$

the averages $\langle * \rangle$ being with respect to all atoms in a subsystem.

From equation (18) it follows that in composites the inner polarization parameter and the participation ratios $\mathcal{R}_1, \mathcal{R}_2$ (that represent the fraction of the total "energy" concentrated on each subsystem) are related. In the zeroth order of the modulation amplitude one has:

$$\mathcal{R}_1 = \frac{\alpha \left\langle |u^{(1)}_{n,g}|^2 \right\rangle}{\alpha \left\langle |u^{(1)}_{n,g}|^2 \right\rangle + \left\langle |u^{(2)}_{m,h}|^2 \right\rangle} \approx \frac{\alpha}{\alpha + t^2} \tag{19}$$

where $t = \frac{1-\beta}{1+\beta}$, $\alpha = a_2/a_1$.

The modes are concentrated on the first subsystem if $\mathcal{R}_1 = 1$, $\mathcal{R}_2 = 1 - \mathcal{R}_1 = 0$. This occurs when $\beta = 1$, $\theta = \gamma_2$, thus when the inner polarization is along the atomic surfaces of the second subsystem. When $\beta = -1$, $\theta = \pi/2$ (inner polarization along the atomic surfaces of the first subsystem) $\mathcal{R}_1 = 0, \mathcal{R}_2 = 1$, hence the modes are concentrated on the second subsystem.

In the above reasoning we supposed that modulation functions are smooth and that $\omega = 0$. We would like to know if $\mathbf{P}$ and β can be defined also elsewhere.

Using group theory reasonings [44] one may show that modes in aperiodic crystals are generalized Bloch waves of the type:

$$u_{n,g,K,y} = \exp[\mathrm{i}K(na_1 + \delta_g)] U_{g,K}[na_1 - y/\tan(\gamma_2)] \tag{20}$$

for modulated crystals

$$\left\{ u^{(1)}_{n,g,K,y}, u^{(2)}_{m,h,K,y} \right\} = \left\{ \begin{array}{l} \exp[\mathrm{i}K(na_1 + \delta^{(1)}_g)] U^{(1)}_{g,K}[na_1 - y/\tan(\gamma_2)], \\ \exp[\mathrm{i}K(ma_2 + \delta^{(2)}_h)] U^{(2)}_{g,K}[ma_2 + y/\tan(\gamma_2)] \end{array} \right\} \tag{21}$$

for composites.

K is the reduced wave vector ($K = k - 2\pi(r/a_1 + s/a_2)$), y is the internal space coordinate (orthogonal to the physical space), γ_2 is the angle in Figure 1 (and $\gamma_1 = \pi/2$). For each value of y one has an equivalent realization of the aperiodic crystal, so one may take $y = 0$ in order to obtain the actual displacements. $U_{g,K}, U^{(1)}_{g,K}, U^{(2)}_{h,K}$ are periodic functions of y, having periods a_2, a_2 and a_1, respectively. We shall call them hull functions and it is useful to picture them in superspace. At $K = 0$, the hull functions play in dynamics the same rôle as the modulation functions play in statics, *i.e.* their intersection with the physical space give the displacements of atoms (Fig. 2). At $K \neq 0$ the hull function displacements are multiplied by sinusoidal plane waves of wavelength $2\pi/K$ (Eqs. (20, 21). Different possible hull functions are represented for modulated crystals in Figure 2. In composites, one should imagine two sets of atomic surfaces and equal polarization vectors $\mathbf{P}$ for the two. As can be understood from Figure 2, the inner polarization can be defined if and only if the atomic surfaces are not distorted. The atomic surfaces are undistorted in a vibration mode if the motion can be described as a rigid motion in superspace. In physical space this comes down to a motion that does not change the local isomorphism class (the set of local atomic configurations remains the same). In the analytic regimes this implies that the hull functions are of the following form:

$$U_{g,K}(y) = \epsilon(K) + \eta(K) \frac{\mathrm{d}f_g}{\mathrm{d}x}(y + \delta_g) \tag{22}$$

$$U^{(1)}_{g,K}(y) = \epsilon(K) + \eta(K) \frac{\mathrm{d}f^{(1)}_g}{\mathrm{d}x} \left[y + \delta^{(1)}_g \right] \tag{23}$$

$$U^{(2)}_{h,K}(y) = \epsilon(K) - \eta(K) - \eta(K) \frac{\mathrm{d}f^{(2)}_h}{\mathrm{d}x} \left[y + \delta^{(2)}_g \right] \tag{24}$$

Equations (22–24) are exact for $K = 0, \omega = 0$ in the analytic regime. We conjecture that they are fulfilled with good accuracy for small K, ω.

In Section 4 we shall check the validity of the undistorted atomic surfaces hypothesis for different models of composite and modulated crystals. For the analysis of these models we shall also need a set of practical formulas to compute parameters $\eta(K), \epsilon(K), \beta(K)$. If equations (22–24) are valid then one has:

$$\epsilon(K) = \langle U_{g,K}(na_1) \rangle \tag{25}$$

$$\eta(K) = \frac{\langle U_{g,K}(na_1) \frac{\mathrm{d}f_g}{\mathrm{d}x}(na_1 + \delta_g) \rangle}{\langle (\frac{\mathrm{d}f_g}{\mathrm{d}x})^2 \rangle} \tag{26}$$

$$\beta(K) = \frac{\eta(K)}{2\epsilon(K) - \eta(K)} = \frac{\langle U_{g,K}(na_1) \frac{\mathrm{d}f_g}{\mathrm{d}x}(na_1 + \delta_g) \rangle}{2\langle (\frac{\mathrm{d}f_g}{\mathrm{d}x})^2 \rangle \langle U_{g,K}(na_1) \rangle - \langle U_{g,K}(na_1) \frac{\mathrm{d}f_g}{\mathrm{d}x}(na_1 + \delta_g) \rangle} \tag{27}$$

for modulated crystals

$$\epsilon(K) = \langle U^{(1)}_{g,K} \rangle \tag{28}$$

$$\eta(K) = \langle U^{(1)}_{g,K} \rangle - \langle U^{(2)}_{h,K} \rangle \tag{29}$$

$$\beta(K) = \frac{\eta(K)}{2\epsilon(K) - \eta(K)} = \frac{\langle U^{(1)}_{g,K} \rangle - \langle U^{(2)}_{h,K} \rangle}{\langle U^{(1)}_{g,K} \rangle + \langle U^{(2)}_{h,K} \rangle} \tag{30}$$

for composite crystals

Several things are worth to be noticed:

– After replacing the displacements by the hull function displacements, *i.e.* after eliminating the sinusoidal plane wave of wavelength $2\pi/K$, $\epsilon(K), \eta(K), \beta(K)$ are

calculated in the same way as they were at $K = 0$ (compare Eqs. (16–18) and Eqs. (27, 30)).
- In modulated crystals, $\epsilon(K)$ is the displacement of the centre of mass and $\eta(k)$ is the linear regression coefficient between the hull function displacements and the derivative of the modulation function.
- In composites, $\epsilon(K)$ is the displacement of the centre of mass of one subsystem and $\eta(K)$ is the relative displacement between the centres of mass of the two subsystems.
- Contrary to the physical polarization which does not change inside a branch, the inner polarization expresses phonon/phason coupling and may depend on K.
- Generally, equations (22–24) are only approximate (atomic surfaces are distorted) and their sum of squares errors [20] are given by:

$$SSE(K) = \sum_{n,g} |U_{g,K}(na_1) - \epsilon(K) - \eta(K)\frac{\mathrm{d}f_g}{\mathrm{d}x}(na_1 + \delta_g)|^2 \quad (31)$$

for modulated crystals

$$SSE(K) = \sum_{n,g} \left|U^{(1)}_{g,K}(na_1) - \epsilon(K) - \eta(K)\frac{\mathrm{d}f^{(1)}_g}{\mathrm{d}x}(na_1 + \delta^{(1)}_g)\right|^2 + \sum_{m,h} \left|U^{(2)}_{h,K}(ma_2) - \epsilon(K) + \eta(K) + \eta(K)\frac{\mathrm{d}f^{(2)}_h}{\mathrm{d}x}(ma_2 + \delta^{(2)}_h)\right|^2 \quad (32)$$

for composite crystals.

Equations (25, 26, 28, 29) provide least squares regression coefficients corresponding to minimum SSE (Eqs. (31, 32)). The inner polarization parameter follows from equations (27, 30).

Traditionally, modes with $\theta = 0$ are called *acoustical phonons*. The name emphasizes the fact that these modes are generic Goldstone modes, occurring in any solid. Modes with $\theta \neq 0$ are usually called phasons, because they involve non-zero phase fluctuations of the modulations. We prefer to call *phason* only the mode whose hull function conserves the center of mass of the solid. In modulated crystals the phason has $\epsilon = 0, \beta = -1, \theta = \pi/2$ corresponding to a vibration of the superspace crystal orthogonal to the physical space, hence along the mean atomic surfaces. The atomic displacements have zero average and conserve the centre of mass. In composites the phason has $\beta = (\rho^{(2)} + \rho^{(1)})/(\rho^{(2)} - \rho^{(1)}), \tan(\theta) = (1 + \rho^{(1)}/\rho^{(2)})\tan(\gamma_2)$ ($\{\rho^{(i)}\}_{i=1,2}$ are the densities of the subsystems) corresponding to a vibration of the superspace crystal in a direction between the average directions of the two sets of atomic surfaces. In the average, the atomic displacements of the subsystems are antiparallel and conserve the overall centre of mass. Of course, there are other possible modes corresponding to arbitrary angles θ. In composites we shall call *sliding modes* all modes with $\eta \neq 0$ (or equivalently $\theta \neq 0, \beta \neq 0$). Because $\eta \neq 0$, sliding modes involve a relative shift between the mass centres of the subsystems. The phason is a particular sliding mode which conserves the overall centre of mass, but there is a continuous set of other possible sliding modes for which the overall centre of mass is not conserved.

The polarization parameter is zero for acoustical phonons (when $\eta = 0$) and may in principle take any non-zero value for mixed phonon/phason modes. In the analytic regime, there are two hydrodynamic branches. The hermiticity of the dynamical matrix imposes the orthogonality of the modes belonging to the two branches, which reads:

$$[1 + \beta^1(K)][1 + \beta^2(K)] + 4\beta^1(K)\beta^2(K)\left\langle (\tfrac{\mathrm{d}f}{\mathrm{d}x})^2 \right\rangle = 0$$

for modulated crystals (33)

$$\{[1 + \beta^1(K)][1 + \beta^2(K)] + \left\langle (\tfrac{\mathrm{d}f^{(1)}}{\mathrm{d}x})^2 \right\rangle\}\rho^{(1)} + \{[1 - \beta^1(K)][1 - \beta^2(K)] + \left\langle (\tfrac{\mathrm{d}f^{(2)}}{\mathrm{d}x})^2 \right\rangle\}\rho^{(2)} = 0$$

for composites. (34)

In the non-analytic regime, the modulation functions are discontinuous and the phason branch has a gap ($\omega^P(K = 0) > 0$). The acoustical phonon ($\beta = 0$) remains the only acoustical branch, and obviously no coupling is possible within the frequency gap (small K), because there is no phason there. Nonetheless, the coupling becomes possible for frequencies $\omega > \omega^P(0)$, leading to crossover phenomena (see Sect. 4). The derivatives of the modulation functions are singular. Hull functions may also become singular in this regime and the equations (22–24) should be understood in the sense of generalized functions. Although this issue deserves further study, it will not be addressed in this paper.

3 Inner polarization and inelastic neutron scattering

Lattice dynamics can be investigated by neutron inelastic scattering.

In coherent neutron inelastic scattering, acoustical modes will be seen as branches issued from main and satellite Bragg reflections, whose positions in reciprocal space (for both modulated and composite crystals) are:

$$k_{r,s} = 2\pi[r/a_1 + s/a_2]. \quad (35)$$

Ignoring damping, the one-phonon inelastic coherent scattering cross-section obeys [9,10]:

$$\left(\tfrac{\mathrm{d}^2\sigma}{\mathrm{d}\Omega \mathrm{d}E}\right)^{inel}_{coh} \sim \sum_p \delta(\omega - \omega^p(K))\tfrac{1}{\omega^p(K)} \times \left|\sum_n \bar{b}_n \exp[-W_n(k)](u^p_n(K)k)\exp(-\mathrm{i}ky_n)\right|^2 \quad (36)$$

where K (already defined in Eqs. (20,21)) is the relative distance to a Bragg peak $k_{r,s}$, *i.e.* $k = k_{r,s}+K$. The index p is for different modes of angular frequency $\omega^p(K)$ and displacements $u_n^p(K)$ in a normalized mode. $\bar{b}_n$ is the average scattering length of the nth atom and $\exp[-W_n(k)]$ is the Debye-Waller factor.

Let us consider that all scattering lengths and Debye-Waller factors are equal. Then, ignoring the frequency dependence $1/\omega^p(K)$ and the slowly varying factor $k\exp[-W_n(k)]$, the following quantity, that we call *dynamical scattering factor*, represents the contribution of one mode to the scattered amplitude along the dispersion branch $\omega = \omega(K)$:

$$DSF(k) = \lim_{N\to\infty} \frac{1}{\sqrt{N}} \sum_{n=1}^{N} u_n \exp(-\mathrm{i}ky_n). \qquad (37)$$

We have considered normal displacements $\sum_{n=1}^{N} |u_n|^2 = 1$. The constant $1/\sqrt{N}$ ensures the convergence of the sum. A pure acoustical phonon mode at $k = 0$ has $u_n = 1/\sqrt{N}$ and $DSF = 1$.

DSF contains information on both structure (*via* the atomic positions y_n) and dynamics (*via* the mode displacements u_n).

The *static structure factor* is:

$$SF(k) = \lim_{N\to\infty} \frac{1}{N} \sum_{n=1}^{N} \exp(-\mathrm{i}ky_n). \qquad (38)$$

In the Appendix we have calculated the SF and the DSF close to a reflection $k_{r,s}$, supposing that equations (22–24) are accurate and that the modulation functions are smooth. It follows that for small modulation amplitudes ($\zeta = k_{r,s} \sup|f| \ll 1$) and for small reciprocal space distances to the reflection ($\chi = |K/k_{r,s}| \ll 1$), the ratio *DSF/SF* depends in lowest order of ζ, χ only on the inner polarization, incommensurability ratio α and indices r, s (see also [17]).

For modulated crystals one has:

$$\left(\frac{|DSF(k_{r,s}+K)|}{|SF(k_{r,s})|}\right)^2 = \frac{1}{1+[1-t(K)]^2\langle(\frac{\mathrm{d}f_g}{\mathrm{d}x})^2\rangle} \left[\frac{\alpha r + t(K)s}{\alpha r + s}\right]^2 \qquad (39)$$

where

$$t(K) = \frac{1-\beta(K)}{1+\beta(K)}\,. \qquad (40)$$

The corresponding relationship for composite crystals is:

$$\left(\frac{|DSF(k_{r,s}+K)|}{|SF(k_{r,s})|}\right)^2 = \frac{n_1\alpha + n_2}{n_1\alpha + n_2 t^2(K)} \left[\frac{\alpha r + t(K)s}{\alpha r + s}\right]^2 \qquad (41)$$

where n_1, n_2 are the numbers of atoms of each subsystem within the periods a_1, a_2, respectively (maximum values of indexes g, h in Eq. (3)).

One should notice that in equation (39–41), $\frac{|DSF|}{|SF|}$ depends on the interaction details only *via* the inner polarization parameter β. For modulated crystals $\langle(\frac{\mathrm{d}f_g}{\mathrm{d}x})^2\rangle$ also depends on the interaction details, but this quantity necessary for the normalization of the modes is the same for all reflections $k_{r,s}$. The K dependence of the ratio $\frac{|DSF|}{|SF|}$ is given by the K dependence of β. This simple result can be used to interpret experimental data, but we should recall that our *DSF* differs from the experimental dynamical structure factor by a factor which depends slowly on k and that we ignored damping.

4 Dynamics of composite crystals using the double chain model

The double chain model was introduced [15,16] in order to study the dynamics of composite structures made of two intermodulated subsystems[2]. This model consists of two parallel chains of atoms. The atoms interact *via* pair potentials and move only longitudinally along the common direction of the chains.

The Hamiltonian of the double chain is:

$$H(p_n^{(1)}, p_m^{(2)}, y_n^{(1)}, y_m^{(2)}) = \sum_n \left[\frac{(p_n^{(1)})^2}{2m_1} + \frac{k^{(1)}}{2}(y_n^{(1)} - y_{n-1}^{(1)} - a_1)^2\right] + \sum_m \left[\frac{(p_m^{(2)})^2}{2m_2} + \frac{k^{(2)}}{2}(y_m^{(2)} - y_{m-1}^{(2)} - a_2)^2\right] + \sum_{n,m} V\left(\frac{y_n^{(1)} - y_m^{(2)}}{r}\right) \qquad (42)$$

where $k^{(1)}$, $k^{(2)}$ and m_1, m_2 are elastic constants and masses for the two chains, and V is the interchain potential of range r.

4.1 Analytic regime

The analytic regime corresponds to weak interaction between the subsystems, or equivalently to rigid subsystems (large $k^{(1)}$, $k^{(2)}$), and is characterized by continuous modulation functions [15].

The dynamical scattering factor for the double chain model with a Gaussian interchain potential ($V(x) = -V_0\exp(-x^2)$) and equal masses $m_1 = m_2$ is shown in Figure 3. Several features may be noticed:

- The dispersion curves of individual chains, touching the $\omega = 0$ axis at the main Bragg reflections, represent the most significant features.
- The intensity maxima form an hierarchical structure.

[2] A similar model was introduced in a different physical context [21].

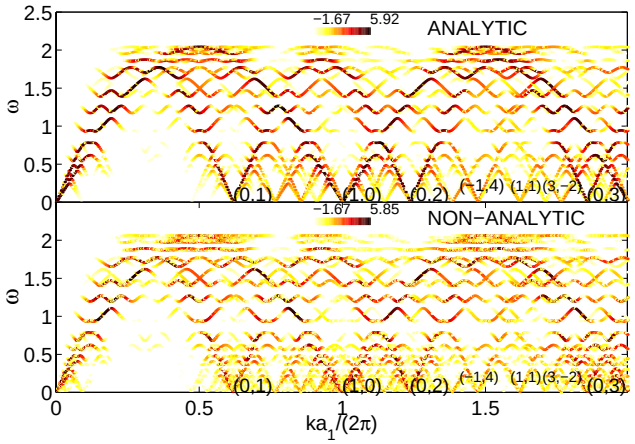

(a)

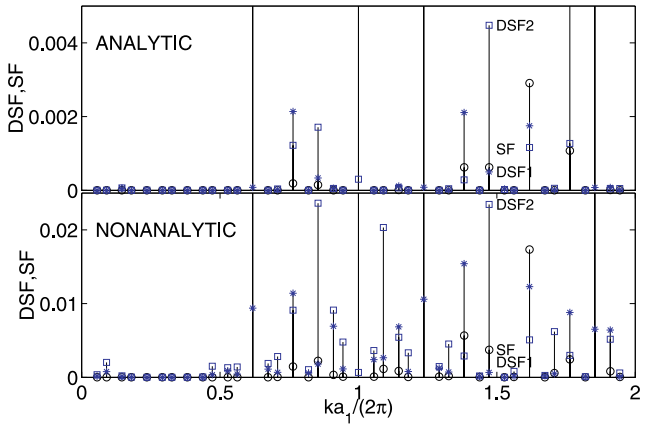

(b)

Fig. 3. a) DSF (DSF1, DSF2 for $\beta = 1, -1$) and SF for the double chain model ($\alpha = (1+\sqrt{5})/2$, $m_1 = m_2$,$k^{(1)}/k^{(2)} = 1.2$, short range Gaussian potential $r = a_1/3$). The calculations were performed on approximants of period $a = pa_1 = qa_2$, $p = 233, q = 144$. Pseudo-colors show DSF values in a logarithmic scale. b) DSF for the two acoustical modes are compared to SF at different reflections. ω is in $\sqrt{k^{(1)}/m_1}$ units.

– From each reflection emerge two branches. One of the acoustical branches is strong at main Bragg reflections $(r, 0)$ and weak at $(0, s)$, while the other branch has the opposite behavior. At satellite positions $((r, s),\ r, s, \neq 0)$, both branches are weak.
– For satellites, strongest *DSF* do not correspond to strongest *SF*. The strongest *DSF* is at $(-1, 4)$, while the strongest SF is at $(1, 1)$.
– At high frequency there are nearly flat bands already observed for the Frenkel-Kontorova model [22] or for the Fibonacci chain quasicrystal model [23].

In order to understand the low frequency aspect of Figure 3 one has first to calculate the inner polarization parameter for the two acoustical branches using equation (27).

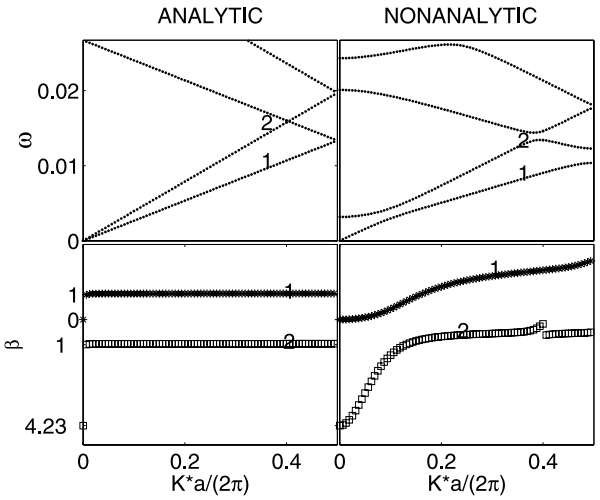

Fig. 4. Lowest frequency branches in the double chain model ($\alpha = (1+\sqrt{5})/2$,$m_1 = m_2$, $k^{(1)}/k^{(2)} = 1.2$, short range Gaussian potential $r = a_1/3$). a) Folded dispersion curves within the first Brillouin zone of the approximant of period $a = pa_1 = qa_2$, $p = 233, q = 144$. ω is in $\sqrt{k^{(1)}/m_1}$ units; b) Inner polarization parameter β along the two branches. Analytic ($k^{(1)}a_1^2/V_o = 60$): concentrated sliding modes ($\beta_1 = 1$,$\beta_2 = -1$). Non-analytic ($k^{(1)}a_1^2/V_o = 25.6$): cross-over from non-concentrated modes (the acoustical phonon $\beta_1 = 0$ and the phason $\beta_2 = -\frac{\alpha+1}{\alpha-1}$) to concentrated sliding modes.

Figure 4 shows the dispersion curves and the inner polarization parameter β for the two acoustic-like branches. The acoustic-like branch 1 is the pure phonon $\beta = 0, \theta = 0$ at $K = 0$ and immediately it becomes a sliding mode concentrated on the first chain ($\beta = 1, \theta = \gamma_2, \mathcal{R}_1 = 1$). At $K = 0$, the acoustic-like branch 2 is the phason with $\beta = (\rho^{(2)} + \rho^{(1)})/(\rho^{(2)} - \rho^{(1)}) = -\frac{\alpha+1}{\alpha-1} \approx -4.23$, $\theta = \tan^{-1}[\tan(\gamma_2)(1+\rho^{(1)}/\rho^{(2)})]$ and at $K \neq 0$ it becomes a sliding mode concentrated on the second chain because $\beta = -1, \theta = \pi/2, \mathcal{R}_1 = 0$. The displacements u_n are shown in Figure 7. The jump of β very close to $K = 0$ is a consequence of the fact that in our numerical simulations we use approximants and thus the phason gap is very small, but not strictly zero. Strictly speaking the inner polarization is undefined at $K = 0$ because of the degeneracy, but in practice there is always a small gap that lifts this degeneracy. Furthermore, although the small K values where the acoustical phonon lives may be inaccessible to neutron inelastic scattering, the above remark is important when determining the speed of sound (this will be $\mathrm{d}\omega/\mathrm{d}K$ for $K = 0, \beta(K) = 0$).

The values of the inner polarization parameter explain why near main Bragg reflections, only one acoustic-like mode is strong (the one concentrated on the chain producing the Bragg reflection) and why the other is much weaker (see also Fig. 5). The mode with $\beta = -1$ is visible near reflections $r = 0$ and the mode with $\beta = 1$ is visible near reflections $s = 0$. This is expressed by equation (41) which has been illustrated in Figure 6. The above behavior of the inner polarization depends on the interchain

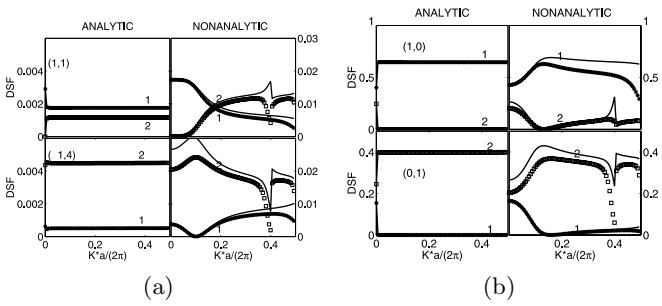

Fig. 5. Numerical values of DSF near the satellites and main Bragg reflections, along the low frequency branches, as a function of the distance in the reciprocal space relative to the reflection. Thick lines were obtained using SF and equation (41). Same parameters as for Figure 4.

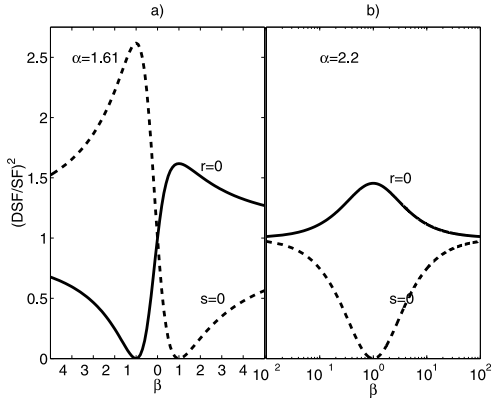

Fig. 6. DSF/SF ratio for the main Bragg reflections of composites as a function of the inner polarization parameter of the mode. a) for $\alpha = (1+\sqrt{5})/2$, as in Figure 4; b) for $\alpha = 2.2$ as in the Bi–2212 lamellar superconductor.

potential and occurs when the slopes of individual dispersion curves of the two chains are not close one to another ($v_1 = \frac{\mathrm{d}\omega_1}{\mathrm{d}K} = a_1\sqrt{\frac{k^{(1)}}{m_1}} \neq v_2 = \frac{\mathrm{d}\omega_2}{\mathrm{d}K} = a_2\sqrt{\frac{k^{(2)}}{m_2}}$). The same inversion of mode intensities between $(r,0)$ and $(0,s)$ main Bragg reflections can be found in Table 1 of [24] for the double chain model with a Lennard-Jones potential.

When the single chain sound velocities v_1, v_2 are close one to another[3], the inner polarization behaves differently. Single chain modes couple strongly and tend to be non-concentrated, involving the participation of both chains ($0 < \mathcal{R}_1 < 1$) and thus contributing to DSF near both types of main Bragg reflections. This type of behavior is illustrated in Figure 8 where we have chosen three different situations: $v_1 = 0.9v_2, v_1 = v_2, v_1 = 1.1v_2$. Although the single chain sound velocities are slightly different in the three cases, after the interaction is set in the dispersion curves look the same; this is the effect of mode repulsion. Nevertheless, the inner polarization parameters reach different values in the three situations. In the case $v_1 = v_2$

[3] The meaning of "how close" depends on the type and range of the interchain potential.

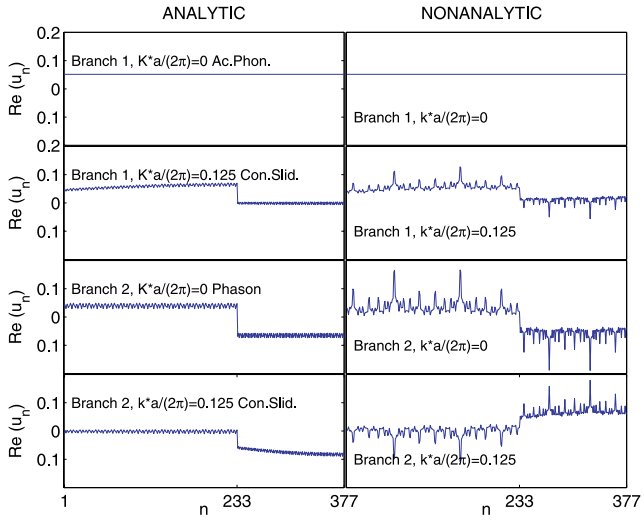

Fig. 7. Lowest frequency modes in the double chain model. Same parameters as for Figure 4. The displacements are longitudinal and correspond to $n = 1, 233$ for the first chain and $n = 234, 377$ for the second chain. They are uniform for the acoustical phonon, antiparallel for the phason and practically involve only one of the two chains for concentrated sliding modes (the other chain presents only the small amplitude rapid oscillations equal to the derivative of the modulation function).

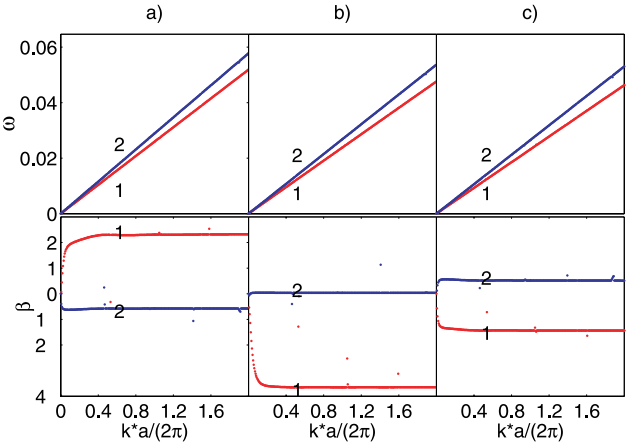

Fig. 8. Unfolded dispersion curves and polarization parameters in the DCM model, when the single chain sound velocities $v_i = a_i\sqrt{k^{(i)}/m_i}$, $i = 1, 2$ are close one to another. a) $v_1 = 0.9v_2$; b) $v_1 = v_2$; c) $v_1 = 1.1v_2$.

one of the branches becomes very close to the pure phason $\beta = -3.58, \mathcal{R}_1 = 0.34$ and the other branch is very close to the acoustical phonon $\beta = 0.04, \mathcal{R}_1 = 0.65$. In the other cases, there are two almost concentrated sliding modes: $\beta = 2.23, \mathcal{R}_1 = 0.92$ and $\beta = -0.58, \mathcal{R}_1 = 0.10$ for $v_1 = 0.9v_2$ and $\beta = 0.52, \mathcal{R}_1 = 0.94$ and $\beta = -1.42, \mathcal{R}_1 = 0.05$ for $v_1 = 1.1v_2$.

Once SF and β known, DSF can be calculated using equation (41). The result is compared to the direct determination of the DSF (*via* Eq. (37)) for wave-vectors close to two satellite reflections in Figure 5. We have checked the validity of equation (41) close to all reflections with $-10 \leq r, s \leq 10$ and the result is illustrated

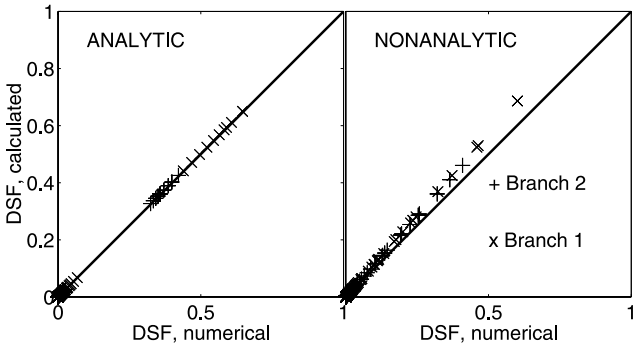

Fig. 9. DCM model: *DSF* obtained directly from equation (37) *vs. DSF* calculated from SF *via* equation (41) for various main and satellite reflections.

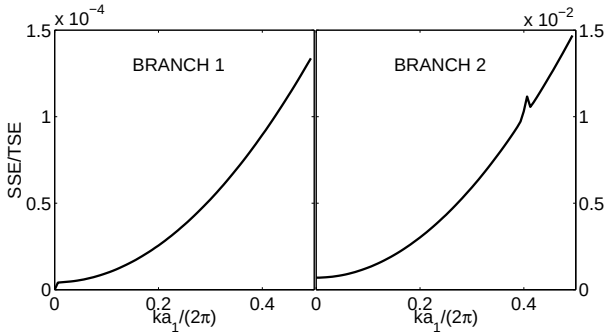

Fig. 10. DCM model: Direct test of equations (23, 24). The ratio *SSE/SST* for the two acoustical branches in the analytic regime is plotted against K. The quality of the regression is excellent ($SSE/SST \ll 1$).

in Figure 9. The very good agreement is a proof that the undistorted atomic surfaces hypothesis is correct at least for large wavelengths. The errors in equation (41) have two origins: eventual deviations from the above hypothesis and the fact that the calculations leading to equation (41) are perturbative and valid for small modulation amplitudes. A direct test of the undistorted atomic surfaces hypothesis is to check equations (22, 23, 24). This is illustrated in Figure 10 where we have plotted the ratio *SSE/SST* against K. *SSE* is the sum of squares error given by equation (32), while SST is the total sum of squares estimating the variance of the hull function ($SST = \sum_n [U^{(1)}(na_1) - \langle U^{(1)} \rangle]^2 + \sum_m [U^{(2)}(ma_2) - \langle U^{(2)} \rangle]^2$). $R = \sqrt{1 - SSE/SST}$ represents the multiple correlation coefficient (R close to 1 means good quality of the linear regression [20]).

4.2 Non-analytic regime

The non-analytic regime occurs when the interaction between the subsystems is strong, or equivalently when the subsystems are soft (small $k^{(1)}$, $k^{(2)}$), and is characterized by discontinuous modulation functions [15]. As a consequence, the phason branch starts with non-zero minimum frequency (gap at $K = 0$). This gap can not be noticed in Figure 3 (it is too small), but it can be seen in Figure 4. Several other gaps exist at higher frequencies and $K \neq 0$.

The variation of β inside the two branches is shown in Figure 4. For low frequencies the branch 1 has $\beta = 0$, hence it is the pure acoustical phonon, while the branch 2 is the phason ($\beta = (\rho^{(2)} + \rho^{(1)})/(\rho^{(2)} - \rho^{(1)})$). This can also be seen in Figure 7 at $K = 0$. The branch 1 corresponds to uniform displacements of the atoms, the branch 2 has the rapid phason oscillations and a sliding character. For higher frequencies both branches are sliding modes, almost concentrated on single chains. Like in the analytic regime, mode concentration can be avoided when the slopes of the individual dispersion curves are similar.

The difference with respect to the analytic case is that the interval of values of K over which the inner polarization changes is much larger (it scales like the gap). A change of the slope $\mathrm{d}\omega/\mathrm{d}K$ accompanies the change of β as can be seen in Figure 4. This could have consequences when different methods of investigation are employed. The speed of sound determined by ultrasound and light Brillouin scattering in the $K = 0$ limit measurements may be different from the slopes $\mathrm{d}\omega/\mathrm{d}K$ determined by neutron measurements.

Although the static structure factor is different from that in the analytic regime, the ratio $|DSF/SF|$ is still given with reasonable accuracy by equation (41). This is shown in Figure 5 where the numerical DSF, and the DSF calculated from SF *via* the equation (41) are compared for two satellite reflections. The accuracy of equation (41) was tested for all reflections (r, s) with $-10 \leq r, s \leq 10$. The result is presented in Figure 9.

To summarize, in both analytic and non-analytic regimes, low frequency features (intensity of acoustical branches close to different reflections) of DSF depend on the SF and on the value of the polarization parameter β. Both SF and β depend on the interaction details of the system, furthermore β may also depend on frequency. For various model parameters and K values, β scans a broad domain of values, corresponding to inner polarizations of various inclinations θ within $(-\pi/2, \pi/2]$.

5 Dynamics of modulated crystals via the DIFFOUR model

DIFFOUR (discrete frustrated Φ^4) models simulate [25] displacively modulated crystals with competing interactions. A simple example is represented by a chain of atoms in positions y_n such that the potential energy depends non-linearly on the fluctuations $x_n = y_n - y_{n-1} - a_1$ of the first neighbor distances. The Hamiltonian is:

$$H(p_n, y_n) = \sum_n \left(\frac{p_n^2}{2m} + \frac{A}{2} x_n^2 + \frac{1}{4} x_n^4 - B x_n x_{n-1} + C x_n x_{n-2} \right). \quad (43)$$

For $A > A^* = B^2/(4C) + 2C$ the ground state is not modulated ($x_n = 0$). Modulation occurs for $A \leq A^*$

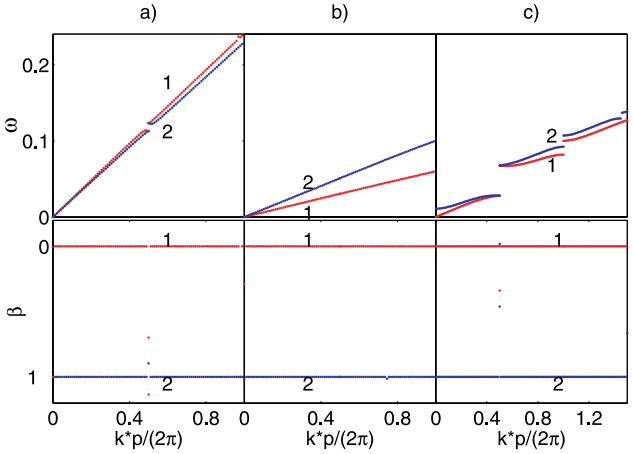

Fig. 11. DIFFOUR model: Unfolded dispersion curves and polarization parameters. We used periodic boundary conditions $pa_1 = qa_2$. a) $C = 0.4$, $A = 0.99A^*$, $B = -2.1C$, $p = 50, q = 17$, analytic regime. b) $C = 0.4$, $A = 0.99A^*$, $B = 2.5C$, $p = 50, q = 7$, analytic regime. c) $C = 0.4$, $A = 0.65A^*$, $B = 2.5C$, $p = 50, q = 7$, non-analytic regime.

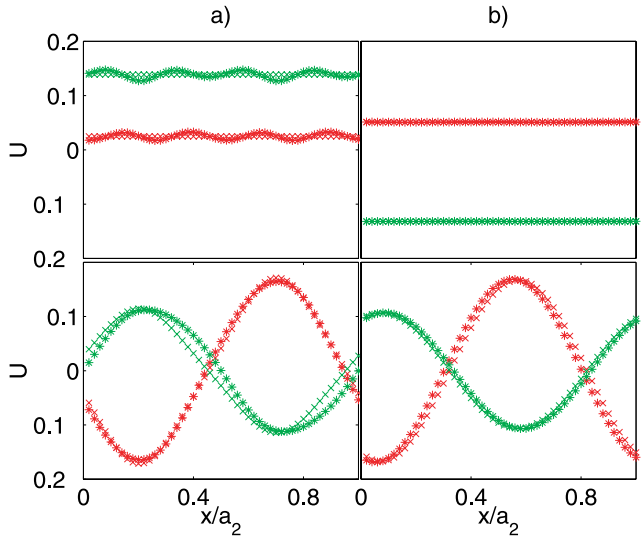

Fig. 12. DIFFOUR model: real (dark) and imaginary (light) parts of the actual (*) and predicted (×) (by Eq. (22)) hull functions for the phonon (up) and for the phason (down) at $K = 0.8\frac{2\pi}{p}$. a) $C = 0.4$, $A = 0.99A^*$, $B = -2.1C$, $p = 50, q = 17$ analytic regime. b) $C = 0.4$, $A = 0.99A^*$, $B = 2.5C$, $p = 50, q = 7$ analytic regime.

with a periodicity a_2 that can be incommensurate to the periodicity a_1 of the basic structure: $a_2 = 2\pi a_1/Q$, where $Q = \arccos(\frac{B}{4C})$. Close to the commensurate-incommensurate (C-IC) transition the modulation is analytic ($A \approx A^*$). Analyticity breaks (the modulation function becomes discontinuous) when A becomes too small. For $A \approx A^*$, the slopes of the hydrodynamic branches are given by $\frac{\mathrm{d}\omega}{\mathrm{d}K} = \{\frac{1}{m}[(2B + A + C)\cos K - 4(2C + B)\cos 2K + 9C\cos 3K]\}^{-1/2}$, with $K = 0$ for the acoustical phonon and $K = Q$ for the phason. These slopes are equal $\left(\frac{\mathrm{d}\omega}{\mathrm{d}K}\right)_{phonon} = \left(\frac{\mathrm{d}\omega}{\mathrm{d}K}\right)_{phason} = 3\sqrt{\frac{C}{m}}$ when $B = -2C$.

In Figure 11 we have represented the dispersion curves and the inner polarization parameter $\beta(K)$ in three situations: $\left(\frac{\mathrm{d}\omega}{\mathrm{d}K}\right)_{phonon} \approx \left(\frac{\mathrm{d}\omega}{\mathrm{d}K}\right)_{phason}$ for an analytic modulation, $\left(\frac{\mathrm{d}\omega}{\mathrm{d}K}\right)_{phonon} \neq \left(\frac{d\omega}{\mathrm{d}K}\right)_{phason}$ for an analytic and a non-analytic modulation. In all these situations β is constant and equal to 0 for the acoustical phonon and is equal to -1 for the phason. No visible phonon/phason coupling occurs. Further insight is given by the hull functions (Fig. 12). With very good accuracy the phason hull function is the derivative of the modulation function and has thus $\beta = -1$. The acoustical phonon corresponds to uniform displacements of the atoms. A small amplitude modulation (though with a wavelength that is a fraction of a_2, hence different from the derivative of the modulation function) add to them when phonon and phason dispersion curves are close (Fig. 12a)).

The DIFFOUR model, like the DCM model, fits to our general scheme and satisfies the non-distorted atomic surfaces condition. Contrary to the DCM model, the values of the inner polarization parameters are practically restricted to $\beta_1 = 0$ and $\beta_2 = -1$, corresponding to the acoustical phonon and to the phason. The following simple argument suggests that close to the C-IC transition the phason/phonon coupling vanishes not only for the DIFFOUR model but for modulated crystals in general. Considering that the potential energy is $\sum_{m,n} V(y_n - y_m)$, that close to the transition the modulation is sinusoidal and of small amplitude, that phonon displacements are $u_n \sim \exp(\mathrm{i}kna_1)$ and that phason displacements are $v_n \sim f'(na_1)\exp(\mathrm{i}kna_1) \sim \exp[\mathrm{i}(k + 2\pi/a_2)na_1]$, then the phason/phonon coupling scales like $\sum_{m,n} u_n^* V''(na_1 - ma_1)v_m \sim \sum_m \exp(2\pi\mathrm{i}ma_1/a_2) = 0$.

6 Composites vs. modulated crystals

Is it possible to distinguish between composites and modulated crystals by studying their dynamics? A possible experimental procedure would be to scan *DSF* in the neighborhood of the main or satellite reflections. One may choose a set of reflections and determine the ratio $|DSF/SF|$ for the acoustical modes. From equations (39, 41) it follows that the dependence of the $|DSF/SF|$ ratio on the reflection indexes r, s has the same form for modulated and composite crystals. The only way to distinguish between different classes of aperiodic crystals is via the polarization parameters. We have shown that these are different for modulated and composite crystals.

First of all, the orthogonality relations (33, 34) that relate inner polarizations of the acoustical modes read differently for the two classes. For instance a $\beta_1 = -1, \theta_1 = \pi/2$ mode (phason in modulated crystals and concentrated sliding mode in composites) is accompanied by a $\beta_2 = 0, \theta_2 = 0$ (acoustical phonon) in modulated crystals and by a $\beta_2 = 1, \theta_2 = \gamma_2$ mode (concentrated sliding mode) in composites. The $\beta_2 = 0$ and $\beta_2 = 1$ modes scatter very

differently and this should be seen in neutron inelastic scattering experiments.

On the other hand, close to the C-IC transition, the inner polarization of normal modes in modulated crystals is restricted to $\beta_1 = -1$ (phason) and $\beta_2 = 0$ (acoustical phonon). Although the numerical simulations using the DIFFOUR model showed only negligible phason/phonon coupling, the theoretical arguments that we employed do not exclude the possibility of a phason/phonon coupling far from the C-IC transition, for instance in the non-analytic regime. In composites, various inner polarizations are possible.

Let us see how the above theoretical considerations can be used to interpret available experimental results on structure and dynamics of incommensurate modulated and composite crystals.

Incommensurate modulated crystals have been studied rather intensively and there are some well characterized model systems [26–29].

For the incommensurate compound $ThBr_4$ [30] the modulation function is analytic, almost sinusoidal (only first order satellites are visible). In this case there is no difficulty to identify the main reflections and the classification task is trivial. A gapless phason was observed by inelastic neutron scattering close to the first order satellite $(2, 3, 0.69)$ of the main Bragg $(2, 3, 1)$. Despite that the intensity of the studied satellite reflection is strong, the acoustical phonon branches were measured only around the main reflections.

In the phase III of biphenyl [26] one can observe strong satellites, up to order 3 in neutron scattering, suggesting a non-analytic (soliton) regime or (which is equivalent) a higher-order commensurate phase. Coherent inelastic neutron scattering scans around a first-order satellite have revealed a frequency gap in the phason branch at $K \neq 0$. The presence of a $K = 0$ gap that would be expected in the non-analytic regime has not been detected, perhaps because of the instrumental resolution and the heavy damping of these excitations.

There are many structures that can be named "composites". Still, a precise classification is not established yet.

The best studied composite system is the mercury chains compound $Hg_{3-\delta}AsF_6$ with $\delta \approx 0.18$ [31,32]. In this case there is no doubt that the structure is composite, being made of two weakly interacting subsystems. The tetrahedra of AsF_6 form the host tetragonal subsystem. There are two mercury subsystems in two orthogonal sets of channels of the host, running along the equivalent incommensurate a and b axes of the tetragonal system. At room temperature the host main Bragg peaks are easily recognizable at positions (h, k, l) and mercury chains produce diffuse thin sheets at $(n(3-\delta), k, l)$ orthogonal to a^* and at $(h, n(3-\delta), l)$ orthogonal to b^*. Near main Bragg peaks of the host and along the incommensurability direction a, acoustical longitudinal modes with a speed $\frac{d\omega}{dK} = 2130\,\mathrm{ms}^{-1}$ were measured. Near mercury chain diffuse sheets and along the same direction a gapless longitudinal branch was measured with a very different speed $\frac{d\omega}{dK} = 3616\,\mathrm{ms}^{-1}$. According to our discussion this suggests the existence of two acoustic-like modes with inner polarization parameters $\beta_1 = 1$ and $\beta_2 = -1$, concentrated on the host and on the mercury chains, respectively. This picture is consistent with the weak inter-subsystem coupling and the large difference between slopes of the dispersion curves (Figs. 4, 5).

The alkane/urea inclusion compounds [33] are also guest/host type composites with two easily recognizable subsystems. At all studied temperatures, guest chains (alkane) have only 1D order and produce diffuse sheets, like in the case of mercury chains, but the alkane modulation is found to be strongly non-harmonic [36,37]. There are no complete studies of dynamics for this compound, nevertheless special features of the longitudinal phonons along the incommensurability direction were observed near main Bragg reflections of the host by neutron scattering [34] and confirmed by Brillouin scattering [38]. These phonons have unusually large damping (approx. 400 GHz, independent of K [35]) compared to the other acoustical phonons (damping scaling like K^2) that could be explained by a sliding character (finite β, phason/phonon coupling). Although this was not studied in this paper, some authors [13,14] suggest that damping and sliding are connected via internal friction. This internal friction can have an intrinsic origin (occurring for large relative velocities [39]) or an extrinsic one (due to defects).

The case of Bi–2212 lamellar superconductor is more complex because there is no clear separation of the subsystems and the structural classification is still controversial [7,40]. Neutron inelastic scattering [8] showed the presence of two longitudinal acoustical branches close to two strong reflections and along the incommensurability direction. The slopes of the dispersion curves are $\frac{d\omega}{dK} = 2\,400$ and $5\,900\,\mathrm{ms}^{-1}$ and their intensities do not change when one passes from one reflection to another. According to equations (39–41) $(DSF/SF)^2_{(0,s)}/(DSF/SF)^2_{(r,0)} = t^2$ irrespective of the type of structure, hence t^2 should be close to 1 for both acoustical branches. This is possible only if $|\beta_1| \ll 1$ and $|\beta_2| \gg 1$. One could not speak of a modulated structure, because this contradicts equation 33. If one of the modes is the acoustical phonon ($\beta_1 = 0, t_1 = 0$) then in modulated crystals the other mode must be the phason ($\beta_2 = -1, t_2 = \infty$) being thus invisible close to main Bragg peaks ($s = 0$). In reference [7] it was assumed that the structure is composite and that the two reflections are the main Bragg peaks $(2, 0)$ and $(0, 1)$. The intensity ratios are compatible with equation (34) and can be explained by considering that one of the longitudinal modes is the acoustical phonon ($\beta_1 = 0$) and that the second is the phason ($|\beta_2| = \frac{\rho^2+\rho^1}{|\rho^2-\rho^1|} = 134.33 \gg 1$ (this was computed considering that the densities for the subsystems $Sr_2CaCu_2O_6$ and $Bi_2O_{2.21}$ are $3.248\ \mathrm{g/cm^3}$ and $3.2\ \mathrm{g/cm^3}$ respectively). For both the above inner polarizations the *DSF/SF* ratio is not changing between the $r = 0$ and the $s = 0$ Bragg reflections (Fig. 6b)). To conclude, dynamics suggests that the superconductor is composite, but the modes are non-concentrated, which is different from the

case of mercury chains compounds. This situation is reproduced by the DCM model in the rather special situation when $v_1 \sim v_2$ (Fig. 8). Before deciding which is really the case, further study is needed in order to check how the interaction details (range and type of the inter-chain potential) and the dimensionality (DCM generalizations to 2D, at least) influence the inner polarization. Referring now to the regime, some of the modulation functions used in the structure refinement have large amplitudes and are non-analytic (in particular an occupational modulation is introduced for the oxygen atoms in the BiO layer of the second subsystem), while other modulation functions could be analytic. One may thus think of a situation when the phason gap is below the experimental resolution of 10 GHz. As discussed in Section 4, this hypothesis could also explain the observed discrepancy between the ultrasound measurement of the speed of sound (4 200 ms^{-1}) and the slope of the neutron dispersion curves.

The dynamics of spin ladder compounds $(Sr_{14-x}Ca_x)Cu_{24}O_{41}$ [41] has been very recently investigated [42]. Again two low frequency longitudinal modes (along the incommensurability direction)were observed close to a main Bragg peak of each subsystem CuO_2 (chains) and $(Sr,Ca)_2Cu_2O_3$ (ladders). One mode is acoustic-like (no gap), the other has a gap of 0.35 THz (for $x = 0$) and can propagate also transversally. Interestingly enough, when the latter propagates longitudinally it looses intensity very rapidly with K. Because of the gap, the mode at low frequencies should be the acoustical phonon. The rapid loss of intensity with K of the second mode (the phason) suggests that this one tends to become a sliding mode concentrated on one of the subsystem when K is increasing, like in Figure 5. The orthogonality conditions impose that the acoustical phonon should also change character when K increases, concentrating on the other subsystem. Our theory predicts that the observation (not yet performed) of a Bragg peak belonging to the other subsystem could reveal an opposite behavior of the intensity of the phason (the intensity loss could be slower than the usual $1/\omega^2$ factor present in Eq. (36)). Of course, a more cautious analysis should also include damping effects.

7 Conclusion and discussion

We emphasized the utility of the concept of inner polarization in the description of low frequency excitations in composite and in modulated aperiodic crystals. This concept has a meaning for long wavelengths in the analytic and even weakly non-analytic dynamical regime, generally for small modulation amplitudes. The inner polarization is related to internal degrees of freedom of the aperiodic crystals and should not be looked at as the direction of atom displacements (this is the physical polarization). Modes having different inner polarizations differ by the amplitude of rapid oscillations added to a uniform overall displacement in modulated crystals and also by the "sliding" character and the relative participation of the subsystems in composites. The inner polarization can be defined for modes that do not change the shape of the superspace atomic surfaces. The possible values of the inner polarization parameter β are different in composites and modulated crystals.

In modulated crystals, close to the C-IC transition the phason and the acoustical phonon should be uncoupled.

In composites, the phason and the acoustical phonon can be coupled. We called "sliding-modes" all the modes with $\beta \neq 0$ (the only exception is the acoustical phonon) because they produce a relative shift of the mass centres of the subsystems. The pure phason is a special sliding mode, the only one that conserves the overall mass centre. One can distinguish two extreme types of dynamics in composites: concentrated modes (two sliding modes with $\beta \in \{-1, 1\}$, involving each one displacements of a single subsystem) and non-concentrated modes (the acoustical phonon, the pure phason or other sliding modes involving both subsystems). Crossover is possible from one type of dynamics to another. The variation of the inner polarization and of the participation ratio with the wave vector K is a different phenomenon from the crossover between diffusive and propagating modes discussed in [13,14,43].

The inner polarization of the modes influences the neutron inelastic scattering. For modulated structures the pure phonon is visible near all main Bragg reflection and satellites, but the phason is visible only near satellites. For composites, the "concentrated" modes are visible only near main Bragg reflections of the subsystem on which they are concentrated, or near satellites, "non-concentrated" modes are visible near both types of main Bragg reflections and also near satellites.

The above properties can be used to distinguish between modulated structures and composites and also between the two extreme types of dynamics in composites. More information could be (at least in principle) extracted by an investigation of the satellites. The inner polarization can be determined from the ratio between the dynamical structure factor and the statical structure factor at various reflections. Of course, for more precision one has to consider also the neglected factor $k\exp[-W(k)]$ in the DSF and the effect of damping on the line shape.

In experiments, it is important to know for a given mode the set of satellites where this is visible. A pure phonon scatters strongly near strong satellites. For modulated structures the empirical observation is that the same thing is true for the phason. This can by justified by multiplying equation (39) for $\beta = -1, t = \infty$ and $k^2\exp[-2W(k)]$ where $k \sim (r\alpha + s)$. We get $I \sim s^2|SF|^2\exp[-2W(k)]$, where I is the intensity scattered by the phason. If $|SF|^2$ decreases with s quicker than $1/s^2$, then the first order satellites $s = 1$ are the most intense and correspond to the strongest phason inelastic scattering. For composites, from equation (41) we get:

- for $\beta = -1$ (sliding mode concentrated on the second subsystem) $I \sim s^2|SF|^2\exp[-2W(k)]$;
- for $\beta = 1$ (sliding mode concentrated on the first subsystem) $I \sim r^2|SF|^2\exp[-2W(k)]$;

– for $\beta = \frac{\rho^{(2)}+\rho^{(1)}}{\rho^{(2)}-\rho^{(1)}}$ (pure phason, hence non-concentrated) $I \sim (r - \frac{\rho^{(1)}}{\alpha\rho^{(2)}}s)^2|SF|^2\exp[-2W(k)]$.

We face here a more complex situation. In composites, one can have significant values of the SF, even if r or s are high for satellites of the type $(1, s)$ or $(r, 1)$ (which are first order for the second and the first subsystem, respectively). Concentrated modes ($\beta = \pm 1$) could scatter strongly when r or s are high. In Figure 3 the reflection $(1, 1)$ has the largest SF, still DSF is stronger for $(-1, 4)$ when $\beta = -1$ and for $(2, -1)$ when $\beta = 1$. For the pure phason, there is an extinction rule: this mode is invisible close to satellites satisfying $r = \frac{\rho^{(1)}}{\alpha\rho^{(2)}}s$ (in the DCM model with $m_1 = m_2$ this becomes $r = s$). This type of extinction has been previously reported in theoretical models [19]. Thus, sliding modes may not give the strongest inelastic scattering near the strongest satellites. In a given practical situation one should use equation (41) together with the measured values of $|SF|$ in order to calculate $|DSF|$ and to find out where this is the strongest.

From our discussion of the inner polarization it becomes clear that sentences of the type "this is the phonon mode and this is the phason (or sliding) mode" referring to acoustic-like modes in composites are at least incomplete. Sliding modes may have various inner polarizations and the pure phonon may simply not exist when there are two sliding modes.

Further study is needed in order to extend (or to specify the limits of) the validity of the results presented here, including the cases of large amplitude and occupational modulations. For a better analysis of the experimental results a treatment of damping is necessary.

Appendix

Let us define the following functions:

$$\psi^{(1,2)}_{k,(g,h)}(x) = \exp[-\mathrm{i}kf^{(1,2)}_{(g,h)}(x)] \tag{44}$$

$$\phi^{(1,2)}_{k,(g,h)}(x) = \tfrac{\mathrm{d}f^{(1,2)}_{(g,h)}}{\mathrm{d}x}(x)\exp[-\mathrm{i}kf^{(1,2)}_{(g,h)}(x)] \tag{45}$$

$\psi^{(1)}_{k,g}$ and $\phi^{(1)}_{k,g}$ are periodic of period a_2, while $\psi^{(2)}_{k,h}$ and $\phi^{(2)}_{k,h}$ are periodic of period a_1. Let $\tilde{\psi}^{(1,2)}_{k,(g,h),m}$ and $\tilde{\phi}^{(1,2)}_{k,(g,h),m}$ be the Fourier coefficients of the above functions, such as:

$$\psi^{(1,2)}_{k,(g,h)}(x) = \textstyle\sum_m \tilde{\psi}^{(1,2)}_{k,(g,h),m}\exp(2\pi\,\mathrm{i}\,m\,x/a_{(2,1)}) \tag{46}$$

$$\phi^{(1,2)}_{k,(g,h)}(x) = \textstyle\sum_m \tilde{\phi}^{(1,2)}_{k,(g,h),m}\exp(2\pi\,\mathrm{i}\,m\,x/a_{(2,1)}). \tag{47}$$

Let us consider periodic approximants such that $a_2/a_1 = p/q$, p, q relatively prime integers. The final result will not depend on this periodic boundary condition because at the end we shall impose $p, q \to \infty$, $a_2/a_1 \to \alpha$.

In composites, the zero frequency normalized acoustical modes are:

$$u^{(1)}_{n,g,K} = N^{-1}_{p,q}\left[1 + \beta(K) + 2\beta(K)\frac{\mathrm{d}f^{(1)}_g}{\mathrm{d}x}(na_1 + \delta^{(1)}_g)\right] \times \exp\left[\mathrm{i}K(na_1 + \delta^{(1)}_g)\right] \tag{48}$$

$$u^{(2)}_{m,h,K} = N^{-1}_{p,q}\left[1 - \beta(K) - 2\beta(K)\frac{\mathrm{d}f^{(2)}_h}{\mathrm{d}x}(ma_2 + \delta^{(2)}_h)\right] \times \exp\left[\mathrm{i}K(ma_2 + \delta^{(2)}_h)\right] \tag{49}$$

where

$$N^2_{p,q} = n_1 p\left\{[1+\beta(K)]^2 + 4\beta^2(K)\left\langle\left|\frac{\mathrm{d}f^{(1)}_g}{\mathrm{d}x}\right|^2\right\rangle\right\} + n_2 q\left\{[1-\beta(K)]^2 + 4\beta^2(K)\left\langle\left|\frac{\mathrm{d}f^{(2)}_h}{\mathrm{d}x}\right|^2\right\rangle\right\}$$

n_1, n_2 being the number of atoms per each sub-period. From equation (37) and $k = 2\pi(r/a_1 + s/a_2) + K$ one gets:

$$DSF^{\text{composites}}(k) = N^{-1}(\alpha, \beta(K))\left\{\sum_{g=1}^{n_1}\alpha\Big[(1+\beta(K))\tilde{\psi}^{(1)}_{k,g,s} + 2\beta(K)\tilde{\Phi}^{(1)}_{k,g,s}\Big] + \sum_{h=1}^{n_2}\Big[(1-\beta(K))\tilde{\psi}^{(2)}_{k,h,r} - 2\beta(K)\tilde{\Phi}^{(2)}_{k,h,r}\Big]\right\} \tag{50}$$

where

$$N^2(\alpha,\beta) = \lim_{p,q\to\infty}\frac{N^2_{p,q}(n_1p + n_2q)}{q^2} = (n_1\alpha + n_2)\left\{n_1\alpha\left[(1+\beta)^2 + 4\beta^2\left\langle\left(\frac{\mathrm{d}f^{(1)}_g}{\mathrm{d}x}\right)^2\right\rangle\right] + n_2\left[(1-\beta)^2 + 4\beta^2\left\langle\left(\frac{\mathrm{d}f^{(2)}_h}{\mathrm{d}x}\right)^2\right\rangle\right]\right\}. \tag{51}$$

Similarly, we obtain:

$$SF^{\text{composites}}(k_{r,s}) = \frac{1}{n_1\alpha + n_2}\left[\alpha\sum_{g=1}^{n_1}\tilde{\psi}^{(1)}_{k_{r,s},g,s} + \sum_{h=1}^{n_2}\tilde{\psi}^{(2)}_{k_{r,s},h,r}\right]. \tag{52}$$

In order to obtain the above results we have used the following version of Poisson's sum rule:

$$\lim_{p\to\infty}\frac{1}{p}\sum_{n=1}^{p}f(naq/p)\exp(-2\pi\,\mathrm{i}nsq/p) = \tilde{f}_s \tag{53}$$

that is valid for any continuous function f, periodic of period a. In order to prove equation (53) one could use

$f(x) = \sum_s \tilde{f}_s \exp(2\pi\,\mathrm{i}\,sx/a)$ and $\sum_{n=1}^{p} \exp[2\pi \mathrm{i} nmq/p] = p\sum_k \delta_{m,kp}$, valid for m, p, q integers p, q relatively prime.

For small modulation amplitudes $|kf^{(1,2)}| \ll 1$, we can use the following linear approximations of equations (44, 45):

$\psi^{(1,2)}_{k,(g,h)}(x) \approx 1 - \mathrm{i}kf^{(1,2)}_{(g,h)}(x)$, $\phi^{(1,2)}_{k,(g,h)}(x) \approx \frac{\mathrm{d}f^{(1,2)}_{(g,h)}}{\mathrm{d}x}$, $\tilde{\psi}^{(1)}_{k,g,s} \approx \delta_{s,0} - \mathrm{i}k\tilde{f}^{(1)}_{g,s}$, $\tilde{\phi}^{(1)}_{k,g,s} \approx \frac{2\pi\mathrm{i}s}{a_2}\tilde{f}^{(1)}_{g,s}$, $\tilde{\psi}^{(2)}_{k,h,r} \approx \delta_{r,0} - \mathrm{i}k\tilde{f}^{(2)}_{h,r}$, $\tilde{\phi}^{(2)}_{k,h,r} \approx \frac{2\pi\mathrm{i}r}{a_1}\tilde{f}^{(2)}_{h,r}$. Substituting in equations (50, 52) one gets:

$$DSF^{\text{composites}}(k) = N^{-1}(\alpha, \beta(K))\Big\{\alpha n_1[1+\beta(K)]\delta_{s,0} + n_2[1-\beta(K)]\delta_{r,0} - \mathrm{i}K\beta(K)F^{-}_{r,s,\alpha} - \mathrm{i}[2\pi(1+\beta(K))\frac{r}{a_1} + 2\pi(1-\beta(K))\frac{s}{a_2} + K]F^{+}_{r,s,\alpha}\Big\} \quad (54)$$

$$SF^{\text{composites}}(k_{r,s}) = \frac{1}{n_1\alpha + n_2}\left[\alpha n_1\delta_{s,0} + n_2\delta_{r,0}\right] - 2\pi i(\frac{r}{a_1} + \frac{s}{a_2})F^{+}_{r,s,\alpha} \quad (55)$$

where

$$F^{\pm}_{r,s,\alpha} = \alpha\sum_{g=1}^{n_1}\tilde{f}^{(1)}_{g,s} \pm \sum_{h=1}^{n_2}\tilde{f}^{(2)}_{h,r}. \quad (56)$$

The same kind of arguments were used for modulated crystals to obtain:

$$DSF^{\text{modulated}}(k) = \left[|\epsilon(K)|^2 + |\eta(K)|^2\left\langle\left(\frac{\mathrm{d}f_g}{\mathrm{d}x}\right)^2\right\rangle\right]^{-1/2} \times\{\epsilon(K)\delta_{s,0} - \mathrm{i}[\epsilon(K)(K + 2\pi\tfrac{r}{a_1}) + (\epsilon(K) - \eta(K))2\pi\tfrac{s}{a_2}]\langle\tilde{f}_{g,s}\rangle\} \quad (57)$$

$$SF^{\text{modulated}}(k_{r,s}) = \delta_{s,0} - 2\pi\mathrm{i}(\tfrac{r}{a_1} + \tfrac{s}{a_2})\langle\tilde{f}_{g,s}\rangle \quad (58)$$

where $\langle\tilde{f}_{g,s}\rangle = \frac{1}{n_1}\sum_{g=1}^{n_1}\tilde{f}_{g,s}$.

References

1. A. Janner, T. Janssen, Acta Cryst. A **36**, 408 (1980)
2. A. Janner, T. Janssen, Rev. Adv. Phys. **36**, 519 (1987)
3. P. Coppens, Acta Cryst. A **47**, 210 (1995)
4. T. Janssen, Phys. Rep. **168**, 55 (1988)
5. V. Petricek, Y. Gao, Y. Lee, P. Coppens, Phys. Rev. B **42**, 387 (1990)
6. V. Petricek, K. Maly, Acta Cryst. A **47**, 210 (1991)
7. J. Etrillard, Ph. Bourges, C.T. Lin, Phys. Rev. B **62**, 150 (2000)
8. J. Etrillard, Ph. Bourges, H.F. He, B. Keimer, B. Liang, C.T. Lin, Europhys. Lett. **55**, 201 (2001)
9. G.L. Squires, *Introduction to the theory of thermal neutron scattering* (Cambridge University Press, Cambridge, 1978)
10. W. Marshall, S.W. Lovesey, *Theory of thermal neutron scattering I* (Clarendon Press, Oxford, 1971)
11. V.J. Emery, J.D. Axe, Phys. Rev. Lett. **40**, 1507 (1978)
12. J.D. Axe, P. Bak, Phys. Rev. B **26**, 4963 (1982)
13. W. Finger, T.M. Rice, Long-wavelength phonons in incommensurate systems, Phys. Rev. B **28**, 340 (1983)
14. R. Currat, E. Kats, I. Luk'yanchuk, Eur. Phys. J. B **26**, 339 (2002)
15. O. Radulescu, T. Janssen, Phys. Rev. B **60**, 12737 (1999)
16. O. Radulescu, T. Janssen, J. Phys. A **30**, 4199 (1997)
17. O. Radulescu, Ferroelectrics **250**, 43 (2001)
18. S. Aubry, G. André, Ann. Israel Phys. Soc. **3**, 133 (1980) Reprinted in *The Physics of Quasicrystals*, edited by P.J. Steinhardt, S. Ostlund (World Scientific, Singapore 1987)
19. T. Janssen, Ferroelectrics **236**, 157 (2000)
20. N. Draper, H. Smith, *Applied Regression Analysis, 2nd edn.* (John Wiley and Sons, Inc., New York, 1981)
21. T. Kawaguchi, H. Matsukawa, Phys. Rev. B **58**, 15866 (1998)
22. N.S. Luo, S.Y. Wu, C.S. Jayanthi, Phys. Rev. B **55**, 11300 (1997)
23. M. Quilichini, T. Janssen, Rev. Mod. Phys. **69**, 277 (1997)
24. L.A. Brussaard, A. Fasolino, T. Janssen, Phys. Rev. B **63**, 214302 (2001)
25. T. Janssen, J.A. Tjon, Phys. Rev. B **25**, 3767 (1982)
26. H. Cailleau, *Incommensurate Phases in Dielectrics*, Vol. 2, edited by R. Blinc, A.P. Levanyuk, in *Modern problems in condensed matter sciences* (North Holland, 1986), pp. 71
27. R. Currat, T. Janssen, Sol. State Phys. **41**, 201 (1988)
28. H.Z. Cummins, Phys.Rep. **185**, 211 (1990)
29. H. Cailleau, C. Ecolivet, Mat. Sci. Forum **100 & 101**, 367 (1992), edited by A. Meerschaut (Trans. Tech. Publ., Aedermannsdorf, 1992)
30. L. Bernard, R. Currat, P. Delamoye, C.M.E. Zeyen, S. Hubert, R. de Kouchkovsky, J. Phys. C **16**, 433 (1983)
31. J.P. Pouget, G. Shirane, J.M. Hastings, A.J. Heeger, N.D. Miro, A.G. MacDiarmid, Phys. Rev. B **18**, 3645 (1983)
32. I.U. Heilmann, J.D. Axe, J.M. Hastings, G. Shirane, A.G. Heeger, A.G. MacDiarmid, Phys. Rev. B **20**, 751 (1979)
33. M.D. Hollingsworth, K.D.M. Harris, in *Comprehensive Supramolecular Chemistry*, Vol. 6, edited by D.D. MacNicol, F. Toda, R. Bishop (Pergamon, Oxford, 1996)
34. R. Lefort, Ph.D. thesis (University of Rennes 1, Rennes 1998)
35. H. Le Lann, Ph.D. thesis (University of Rennes 1, Rennes 2000)
36. R. Lefort, J. Etrillard, B. Toudic, F. Guillaume, T. Breczewski, P. Bourges, Phys. Rev. Lett. **77**, 4027 (1996)
37. T. Weber, H. Boysen, F. Frey, R.B. Neder, Acta Cryst. B **53**, 544 (1997)
38. J. Ollivier, C. Ecolivet, S. Beaufils, F. Guillaume, T. Breczewski, Europhys. Lett. **43**, 546 (1997)
39. T. Janssen, O. Radulescu, A.N. Rubtsov, Eur. Phys. J. B **29**, 85 (2002)
40. D. Grebille, H. Leligny, O. Perez, Phys. Rev. B **64**, 106501 (2001)
41. E.M. McCarron, M.A. Subramanian, J.C. Calabrese, R.L. Harlow, Mat. Res. Bull. **23**, 1355 (1988)
42. J. Etrillard, M. Braden, work in progress
43. R. Zeyher, W. Finger, Phys. Rev. Lett. **49**, 1833 (1982)
44. T. Janssen, J. Phys. C **12**, 5381 (1979)